buildings

MDPI

Article

Linear and Nonlinear Earthquake Analysis for Strength Evaluation of Masonry Monument of Neoria

Maria E. Stavroulaki [1], Amalia Kasampali [1], Barbara Charalambidi [1], Siphesihle Mpho Motsa [2], Georgios A. Drosopoulos [2,3] and Georgios E. Stavroulakis [4,*]

[1] School of Architecture, Technical University of Crete, 73100 Chania, Crete, Greece; mstavroulaki@tuc.gr (M.E.S.); amalia.kasampali@gmail.com (A.K.); bcharalambidi@gmail.com (B.C.)
[2] Discipline of Civil Engineering, University of KwaZulu Natal, Durban 4041, South Africa; motsampho@gmail.com (S.M.M.); gdrosopoulos@uclan.ac.uk (G.A.D.)
[3] Discipline of Civil Engineering, University of Central Lancashire, Preston PR1 2HE, UK
[4] School of Production Engineering & Management, Technical University of Crete, 73100 Chania, Crete, Greece
* Correspondence: gestavroulakis@tuc.gr; Tel.: +30-282-103-7418

Abstract: An evaluation of the seismic behavior of a massive masonry monument with vaults, namely, the Neoria complex at the old port of Chania, is presented here. The usage of modal response analysis requires the combination of many eigenmodes in order to capture the required amount of vibration energy. Alternatively, a number of earthquakes can be used within a time domain response analysis in order to evaluate the response and, subsequently, the strength of the structure. Results of linear analysis are compared here, since this is what is required from current seismic codes. A nonlinear analysis with adequate material models will also be presented in order to demonstrate a comparison with linear analysis and a prediction of damage appearance under ultimate conditions. From the present investigation, it is shown that the results of the modal analysis and the linear time-step analysis are comparable. Therefore, some confidence is gained towards using the results for the design of strengthening and rehabilitation studies. Nonlinear models are very sensitive with respect to design earthquakes and material models. Therefore, at this stage, their results are used for the identification of areas where interventions must be performed very carefully.

Keywords: finite element analysis; nonlinear time history analysis; earthquake analysis; unreinforced masonry; time-step analysis; masonry vaults; masonry damage

Citation: Stavroulaki, M.E.; Kasampali, A.; Charalambidi, B.; Motsa, S.M.; Drosopoulos, G.A.; Stavroulakis, G.E. Linear and Nonlinear Earthquake Analysis for Strength Evaluation of Masonry Monument of Neoria. *Buildings* **2023**, *13*, 2204. https://doi.org/10.3390/buildings13092204

Academic Editor: Harry Far

Received: 29 July 2023
Revised: 25 August 2023
Accepted: 28 August 2023
Published: 30 August 2023

1. Introduction

Computational modelling of masonry monuments has been the focus of various investigations, due to the complexity of the structures, the uncertainty of materials and the constitutive models [1–4]. The usage of simplified models, and especially of equivalent frame models, is questionable, since the response usually does not capture the complex three-dimensional structure [5–7].

On the other hand, more complicated models, including contact interaction and the influence of the microstructure on the structural behavior, are available, provided that reliable data can be found [8,9]. In these models, sophisticated multi-scale schemes are adopted, coupling the micro- and macroscopic scales. In [10], an alternative probabilistic-based numerical method is proposed, coupling a discrete macro-element model with a homogenization meso-scale model. It is noted that these techniques can accurately describe the microstructure of masonry, but they are usually complex and computationally expensive and, thus, not easily implemented in large masonry structures and monuments.

When the study focuses on large masonry structures, retrofitting and reinforcing must be limited to the minimum necessary due to practical difficulties and the generally accepted trend to avoid heavy interventions in monuments [11]. The nominal life of interventions and the question of cost-benefit analysis is another aspect that should be

taken into account [12]. Hence, to evaluate the structural response and propose specific interventions aiming to preserve masonry structures, numerical studies focusing on their static and dynamic response have been developed in the last years, involving direct finite element simulations on the macroscopic, structural length scale.

In addition, masonry monuments require special attention due to their particular structural characteristics and their cultural significance. Issues such as uncertainty in material properties, existing damage and previous interventions—which should be addressed in every study—make each investigation a unique case study. In [13], a nonlinear time history, finite element analysis is used to investigate how the concrete vault cover, applied to a masonry mosque in previous years, influences the seismic response and the collapse mechanism of the structure. The dynamic response of a bottle-shaped masonry ancient pagoda is evaluated in [14] using the finite element method. The study focuses on identifying seismic weak areas on the structure. In [15], the non-smooth contact dynamics method is used to simulate the nonlinear response of the civic clock tower of Rotella, in Italy. The study provides the failure modes as a parameter of the shape, size and texture of the masonry. A comparative analysis study between discontinuous and continuous models applied to masonry structures is given in [16] for the structural evaluation of an old church subjected to seismic events. More recent studies on numerical methods evaluating the dynamic response of masonry structures and monuments can be found in [17–22].

In this article, the dynamic response of the masonry monument of Neoria in the Venetian Port of Chania (Greece) is evaluated using linear and nonlinear dynamic finite element analysis. For the strength evaluation of the unreinforced structure, a design model was created initially, by a geometric, historic and material survey, which formed the basis for the discretization of the structure using the finite element method, see [23], following the steps outlined in [8,24]. This model allowed for the initial assessment of the mechanical (dynamic) characteristics of the structure and the comparison with the measured (experimental) data. The model was parametrized to a sufficient degree and allowed researchers to consider different scenarios regarding the mechanical properties of the material at different locations, depending on the state of damage, to compare with the measurements of modal characteristics and, finally, to estimate the real state of the structure.

The initial study on the monument presented in [23] led, through parameter identification techniques, to a reliable finite element model of the existing structure. In this paper, we assume that cracks and damages will be restored, and some minor architectural changes will be realized, namely the removal of the front walls, which are not bearing elements of the structure. These interventions and the details of the new finite element model of the monument are provided in subsequent sections. The results of modal and dynamic spectral analysis of this final model, as well as its transient dynamic simulations for old earthquake records, are briefly presented here and critically evaluated in view of rehabilitation and new usage of the monument. A compromise between research investigation and engineering practice is attempted within this paper.

It must be emphasized that all presented investigations are possible due to the usage of advanced finite element analysis. The complex shape of the structure, the need to describe documented damages [23] and the need to use a large number of modes within the modal analysis justifies the usage of modern general-purpose finite elements. This observation is in accordance with many recently published investigations, such as [4,15,16,24,25].

2. Brief Description of Neoria Masonry Monument

The Neoria masonry monument is a shipyard building built in the 16th century. As shown in Figure 1a, the building consists of seven vaults, eight lateral masonry walls, and two facades on the north and south sides. The front (north) façade was originally open for the entry of the ships, and the southern walls were constructed and connected to the lateral walls up to the base of the vaults. The dimensions for each of the seven shipyards of the Neoria building are 50 m $\times$ 9 m. The shape of the floor plan is a stepped trapezoid, as the walls that carry the vaulting are parallel to each other, while the north and south sides

deviate noticeably from the vertical in order to adapt to the morphology of the coastline and the road parallel to it. The width of the aisles is approximately 9.10 m, with the exception of the fourth and seventh, which are approximately 9.20 m wide. The rooms were originally open to the north, from which the boats entered. Their length ranges from 52 m in the first to 47 m in the seventh. The walls between the naves are very thick (1.70–1.90 m) so that they receive the loads of the domes. They have an even greater thickness when they also have to take on lateral thrusts—that is, in the cases where it is the extreme wall towards the east of an array of domes that was roofed at the same time. To this category belong the eastern walls of the first, sixth and seventh neorios, with a thickness of 3.20, 2.60 and 3.25 m, respectively. The wall of the seventh youth is less thick than the height of the genesis of the dome and above. In this way, the dome of the next nave to the west was planned, but it was never built. To deal with the westward thrusts of the dome of the first youth, six massive buttresses were built after the collapse of the westernmost domes in the 19th century. The southern wall is noticeably thinner than the rest (1.00 m and approx. 0.60 m in the fifth new wall) since it does not receive loads from the vaulting.

The building is constructed of cut stones, up to a height of about 2.5 m, and rubblework for the rest of the mass of the walls and the vaults. More details about the structural condition and existing damage of the building can be found in [23]. For the convenience of the readers, major geometric quantities of the structure are reproduced in Figure 1b.

(**a**)

Figure 1. *Cont.*

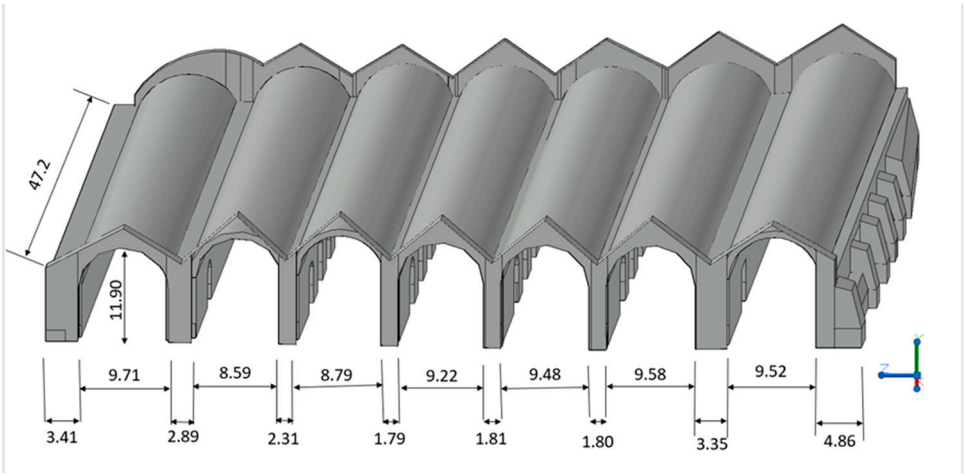

(**b**)

Figure 1. (**a**) Neoria masonry monument; (**b**) dimensions of the building.

2.1. General Description and Material Properties

A detailed finite element model of the structure, which considers the planned strengthening and other interventions, has been created, as shown Figure 2. The main intervention, which is applied in this model as compared to [23], is the removal of the north facade walls, which, notably, were added during the life of the structure and do not contribute to the bearing structural system. Additionally, for strengthening, it is assumed that the masonry structure has been restored by grouting the masonry and repairing the cracks with stone joints.

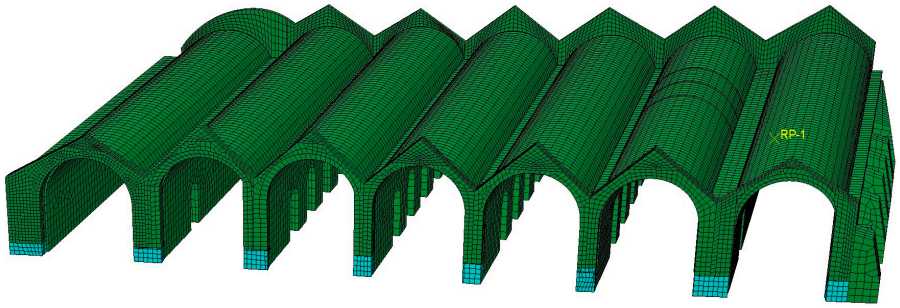

Figure 2. Finite element model of Neoria, considering planned interventions. The current structure is described in [23].

To evaluate the dynamic response, which is obtained from this refined model, dynamic simulations of the structure were carried out by calculating the eigenfrequencies and eigenmodes and then by applying the design spectrum according to the Greek Anti-Seismic Regulation [26]. Next, linear and nonlinear dynamic simulations in the time domain, using natural and fitted earthquakes, which are available through international and national databases, were implemented.

The mechanical properties of the masonry, which have been obtained from the experimental measurements and the parameter identification optimization process described in [1], are shown in Table 1.

For the nonlinear time history analysis, which is one of the simulations conducted to evaluate the ultimate response of the masonry monument under dynamic actions, the concrete damage plasticity law is adopted in commercial finite element software (Abaqus). The concrete damage plasticity model has been used in recent nonlinear analysis studies of monuments [27]. This is a continuum constitutive description, which is appropriate for the simulation of failure on quasi-brittle materials such as masonry and concrete [28].

Table 1. Mechanical properties of materials.

Material	Young's Modulus E ($\times 10^9$ Pa)	Mass Density (kg/m^3)	Poisson's Ratio ν
Vaults	3.43	1900	0.15
South wall	1.50	1500	0.25
Weak walls	3.14	1700	0.25
Strong walls	3.29	1700	0.25

The main two failure mechanisms that can be depicted by this constitutive material law are tensile and compressive failure. Damage variables were introduced in this law to capture the mentioned failure types. The nonlinear material properties that were adopted in these simulations are given in Figure 3.

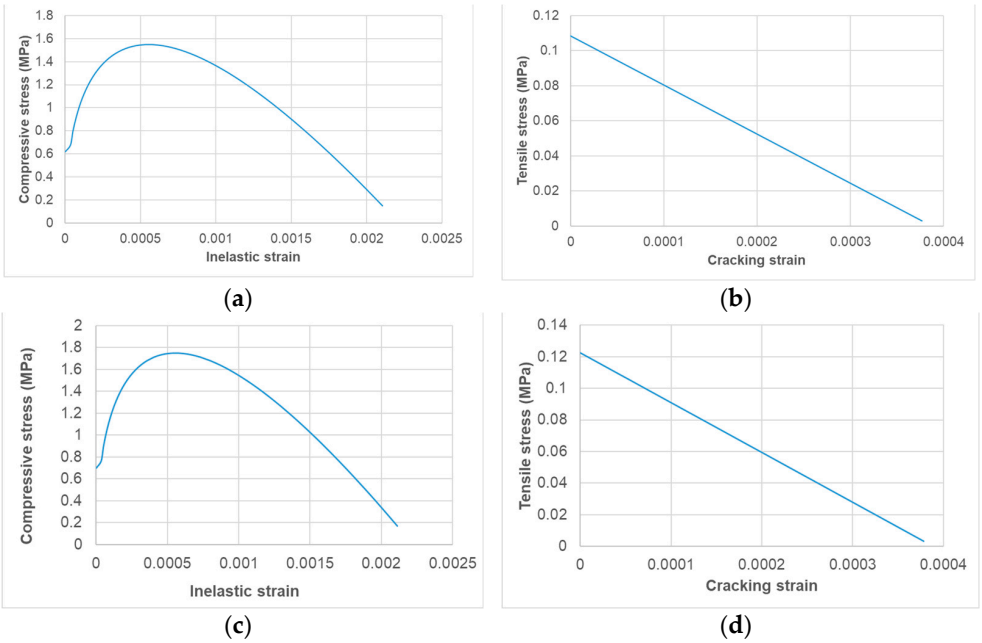

Figure 3. Material laws adopted for the concrete damage plasticity model: (**a**) compressive stress–inelastic strain response for the vaults; (**b**) tensile stress–inelastic strain response for the vaults; (**c**) compressive stress–inelastic strain response for the walls; (**d**) tensile stress–inelastic strain response for the walls.

2.2. Details of the Response Spectrum Analysis

The structure was evaluated with the elastic design spectrum prescribed by the seismic code in the region—following Eurocode 8, part 3, with PGA 0–24 g—as shown in Figure 4, for the following characteristics: ground category B, category of importance III and seismic risk zone Z2. The values of the spectrum were multiplied by an importance factor of 1.3 to capture the worst earthquake loading. The seismic loading was initially considered to act in the three directions in the space, with different participation factors for each direction (e.g., main directions or, alternatively, the two axes of the structure's plan) according to the anti-seismic regulation.

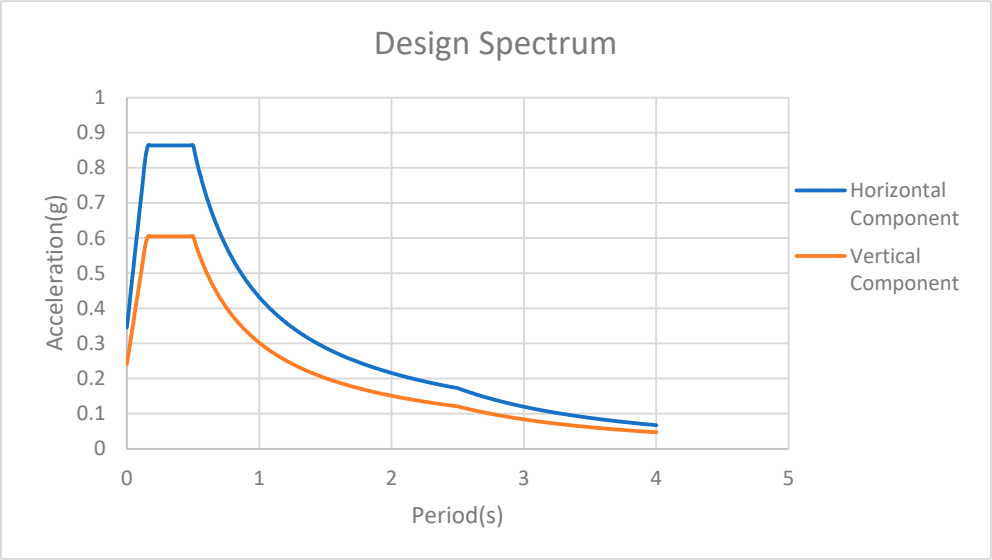

Figure 4. Design spectrum adopted in this study.

2.3. Time History Analysis

The selected earthquakes, which are shown in Table 2, have been scaled to comply with the design spectrum provided in Figure 4. The scaling of the real earthquake ground acceleration diagrams was implemented by using the commercial software Seismosoft [29]. First, the design spectrum is defined, which was applicable in the region as recommended by the Eurocode, according to the descriptions given in Section 3.2. Then, the nonstationary spectral matching algorithm was used [30] to match the real earthquake ground acceleration diagram to the pre-defined design spectrum. It is noted that, according to the Eurocode, the design spectrum for the vertical component of the earthquake acceleration time history data can be equal to 0.7 of the horizontal component.

Table 2. Selected earthquakes (sources: http://www.itsak.gr/db/data/strong_motion/after2000/, https://ngawest2.berkeley.edu/, access on 18 August 2023).

No.	Mw	Event Name	Name of Station	Date of Event
EQ.1	6.3	Thessaly Earthquake	Station S5	3 March 2021
EQ.2	6.3	Thessaly Earthquake	Station S4	3 March 2021
EQ.3	6.0	Arkalochori Earthquake (Main shock)	Station ABEA	27 September 2021
EQ.4	5.3	Arkalochori Earthquake (Secondary shock)	Station ABEA	28 September 2021
EQ.5	6.1	Earthquake West of Chania	Station ABEA	27 November 2019
EQ.6	6.7	Samos Earthquake	Station ABEA	30 October 2020
EQ.7	6.69	Northridge, California	Griffith Observatory	17 January 1994
EQ.8	6.7	Northridge, California	MT Wilson-Cit Seis Station (CDMG Station 24399)	17 January 1994
EQ.9	6.9	Irpinia, Italy	Sturno	23 November 1980

Indicative results of this scaling process from the spectrum of earthquake No. 7, Northridge, California, is shown in Figure 5. The measurement points for plotting the relative displacement diagrams, which are provided in the results, are shown in Figure 6.

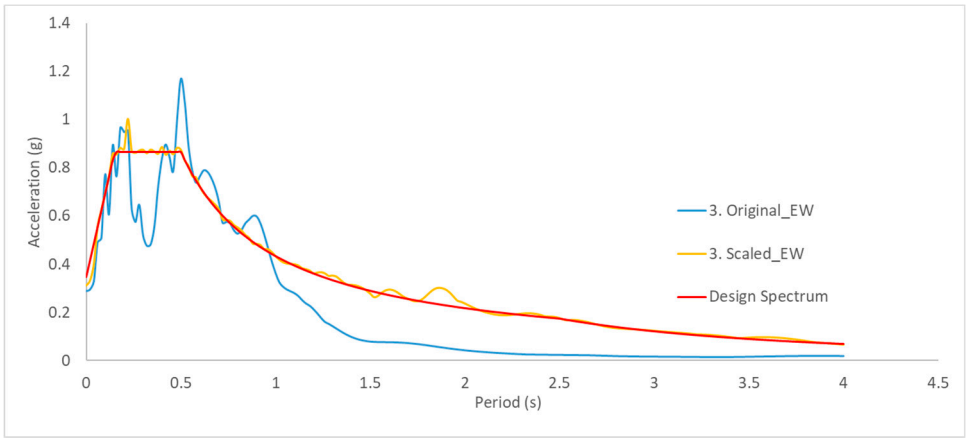

(**a**)

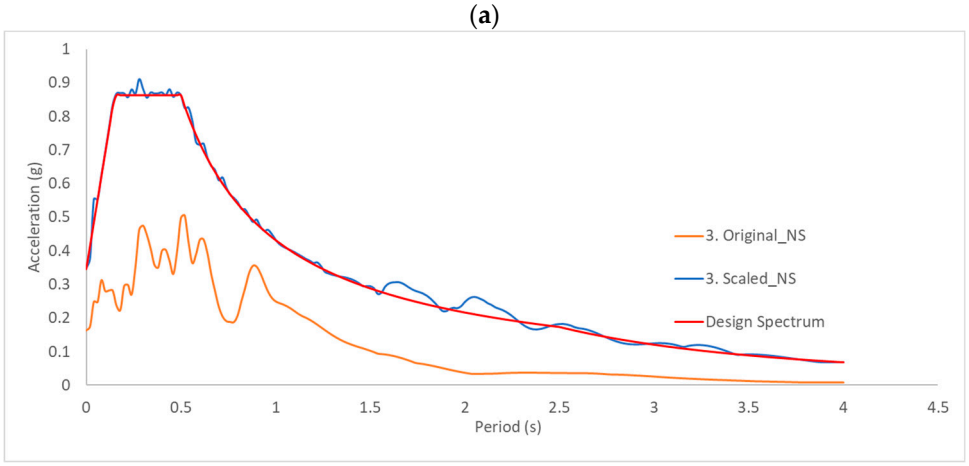

(**b**)

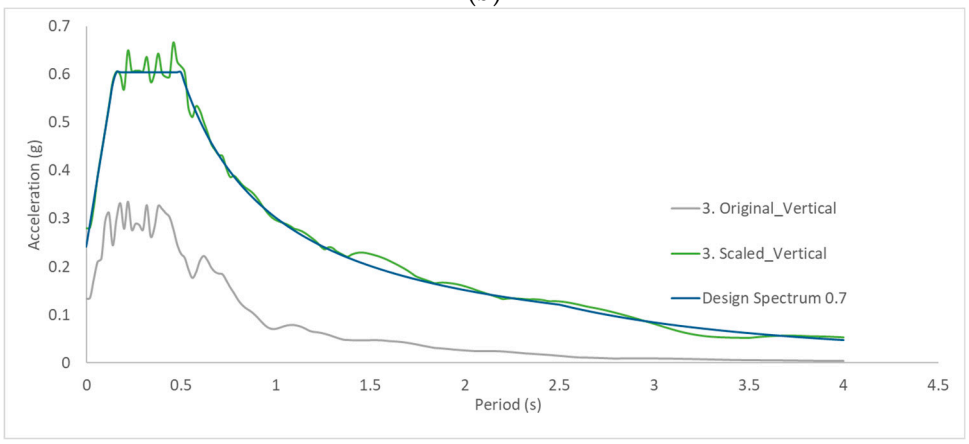

(**c**)

Figure 5. Spectrum of earthquake (Northridge, California) without and with scaling in various directions: (**a**) east–west; (**b**) north–south; (**c**) vertical.

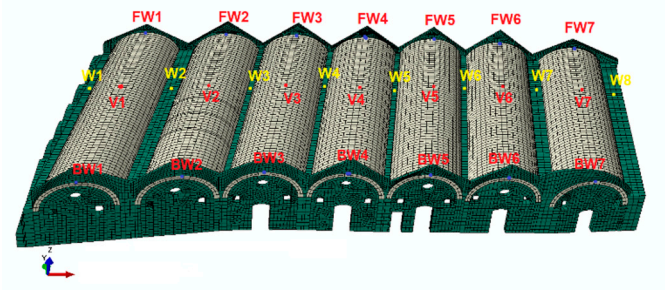

Figure 6. The FEM model of the structure and points on it where displacement time histories have been collected.

Following the scaling of the ground acceleration diagrams for the seismic events shown in Table 2 to fit the design spectrum, scaling of the ground acceleration diagrams to new ground accelerations complying to the design spectrum was considered. In the results section, output from linear time history analysis was provided using these scaled ground accelerations.

Figures 7 and 8 show two scaled ground acceleration diagrams representing the old seismic events of Table 2, namely, the Thessaly and Northridge, California events. In particular, both the original and the scaled ground acceleration loadings corresponding to these events are provided in Figures 7 and 8. These scaled diagrams are used in the results section of the article, to provide the nonlinear response of the monument when nonlinear time history analysis is performed. According to Figures 7 and 8, the scaled ground acceleration values were increased as compared to the original ones. The reason for this increase was to allow the chosen ground accelerations of old seismic events, complying with the design spectrum in the location of the building under investigation. Technical details for the nonlinear analysis for monuments can be found in [8,28].

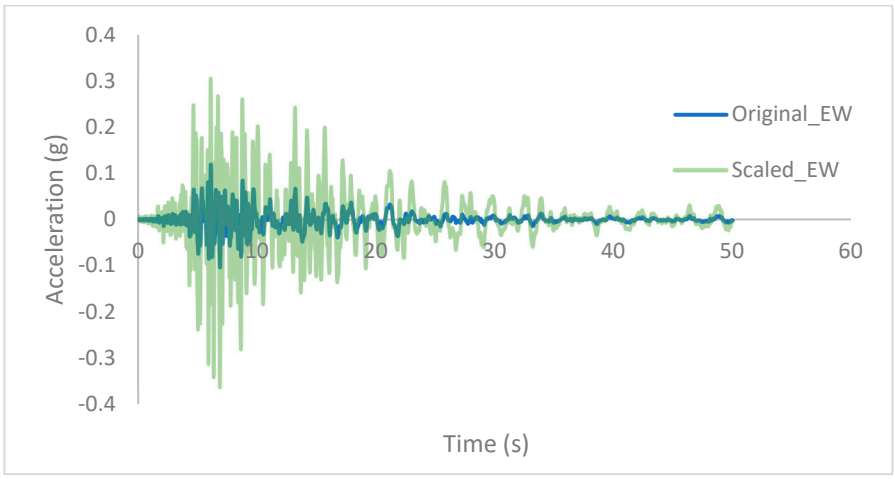

(**a**)

Figure 7. *Cont.*

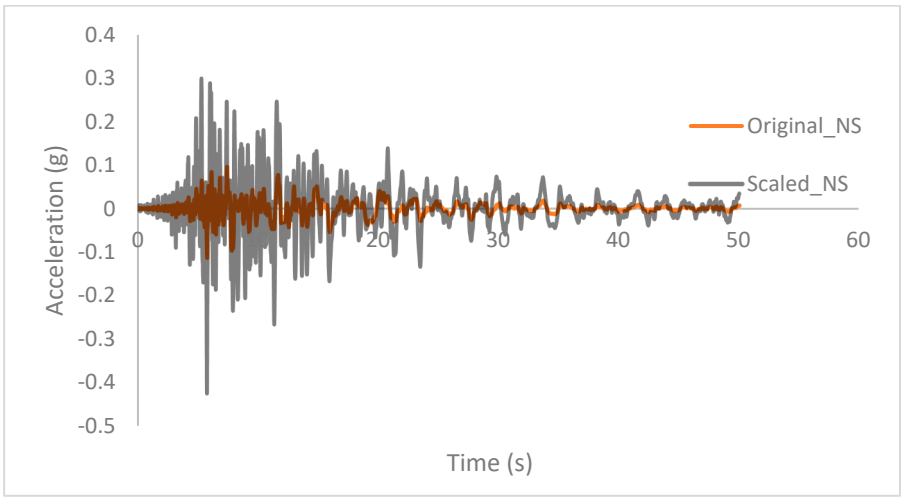

(**b**)

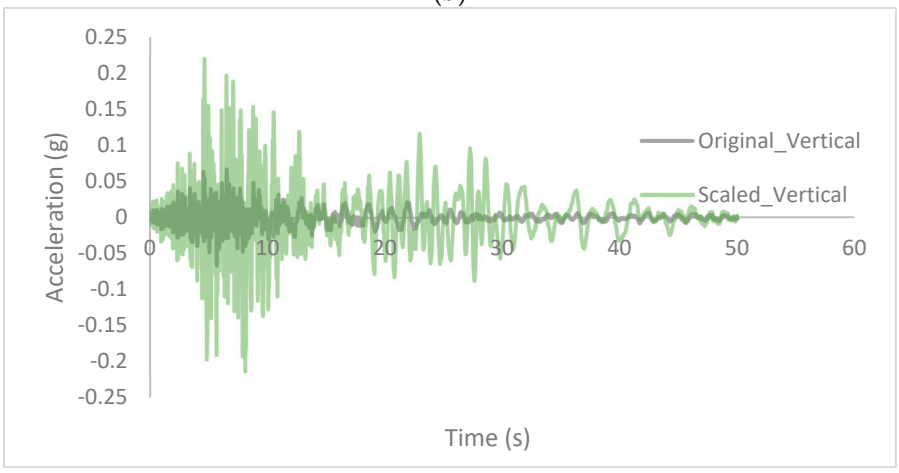

(**c**)

Figure 7. Original and scaled ground acceleration diagrams for the Thessaly seismic event: (**a**) horizontal direction east–west; (**b**) horizontal direction north–south; (**c**) vertical direction.

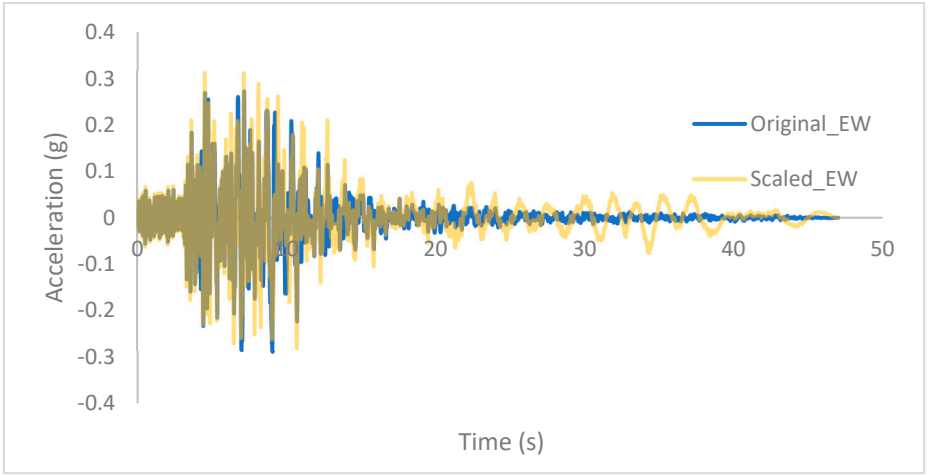

(**a**)

Figure 8. *Cont*.

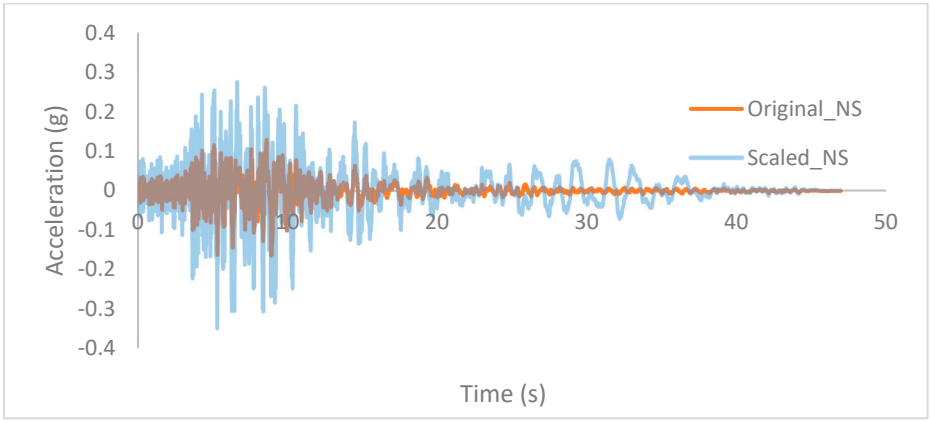

(**b**)

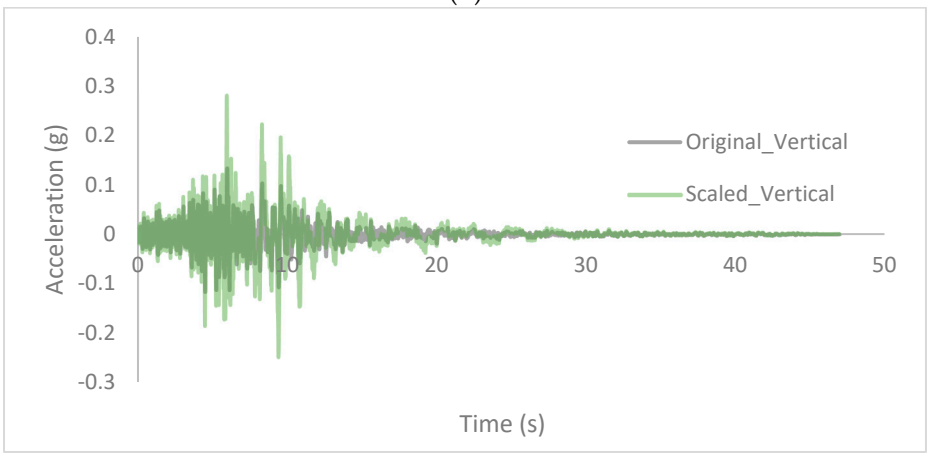

(**c**)

Figure 8. Original and scaled ground acceleration diagrams for the Northridge seismic event: (**a**) horizontal direction east–west; (**b**) horizontal direction north–south; (**c**) vertical direction.

3. Results

To evaluate the dynamic response of the monument, four types of dynamic simulations were implemented: modal analysis, response spectrum analysis and linear and nonlinear time history analysis.

3.1. Modal Analysis

The modal analysis is needed for the investigation of the response of a system to dynamic loading, as it can provide qualitative as well as quantitative estimates for the expected displacements and deformations. This method is a good approximation of the intensive quantities that develop in cases of non-periodic variable loads, such as an earthquake and, by extension, the determination of the most vulnerable points of the structure. The first, third and fifteenth eigenmodes are shown in Figures 9 and 10. In these frequencies, already, the existing structure is excited [23].

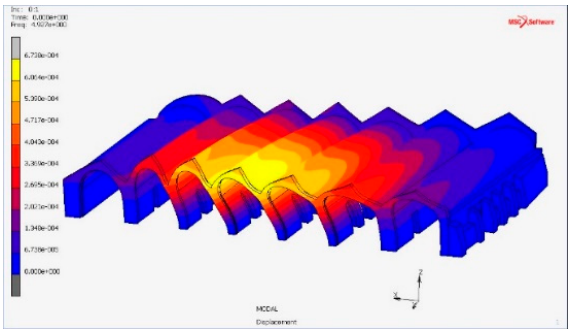

Figure 9. 1st eigenmode at 4927 Hz (north face).

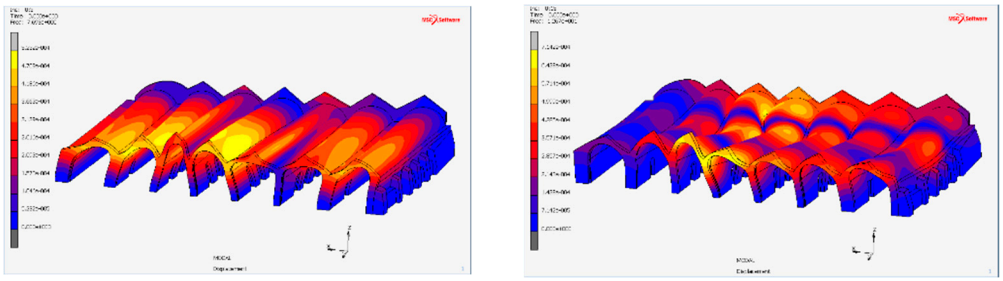

(**a**) (**b**)

Figure 10. (**a**) 3rd eigenmode at 7.693 Hz; (**b**) 15th eigenmode at 12.67 Hz (north face).

3.2. Response Spectrum Analysis

Indicative results of the displacements and principal stresses, which developed in the structure, are shown in Figures 11 and 12, respectively. The distribution of maximum and minimum principal stresses shown in Figure 12 indicate that critical areas were detected in the weak inner walls and in the central vaults.

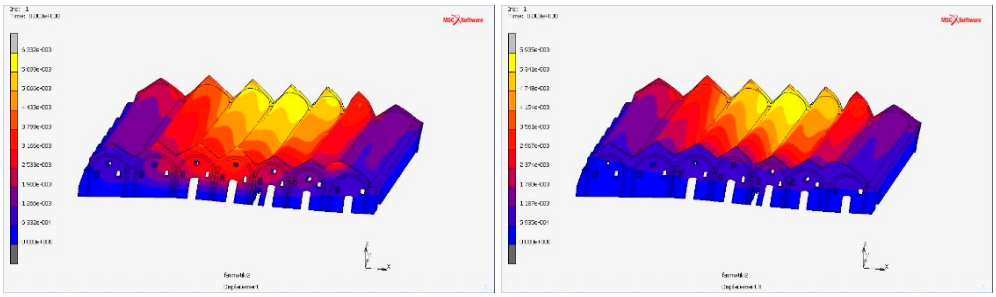

(**a**) (**b**)

Figure 11. (**a**) Total displacement; (**b**) displacement along the x direction, obtained from dynamic spectral analysis (in m).

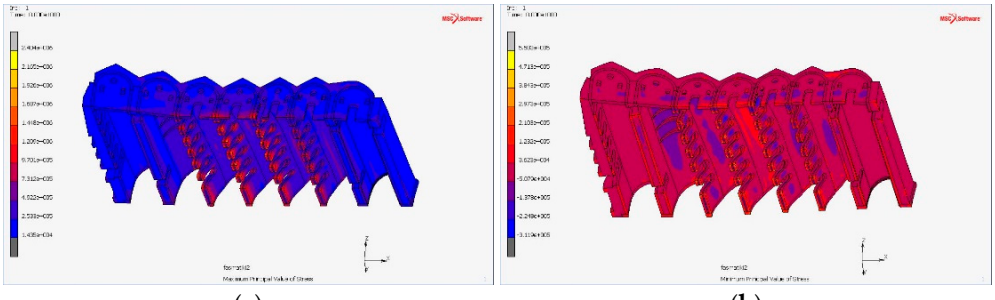

(**a**) (**b**)

Figure 12. (**a**) Maximum; (**b**) minimum principal stress from the dynamic spectral analysis (in Pa).

It is also concluded that the maximum displacement shown in Figure 11 appears at the top of the fourth vault as well as at the pediment projections on the south face. In the vaults, the excitation on the *X* axis has a greater influence. In the south, higher stress concentrations appear in the *Y*-axis stresses, due to out-of-plane bending. The removal of the masonry wall on the north face led to greater oscillations of the free end of the domes. In fact, the existing masonry has largely detached from the domes, so, the effect of the removal has already taken place in the structure with micro-cracks at the ends of the domes on the north side.

It is of note that, during the spectral analysis, the regulations require that as many eigenmodes be used in each component as are necessary to cover 75% of the total mass and, in any case, to consider the eigenmodes with T $\geq$ 0.20 s. For this reason, and in order to follow these requirements, it was found by previous investigations that more than 90 eigenmodes must be used [23]. So, the choice of using time domain solutions for earthquakes seems to be a more reliable alternative.

3.3. Linear Time History Analysis

A time domain finite element analysis has been performed in this section. A sample set of response displacements at a point on the fourth vault of the structure is shown in Figure 13, for the selected earthquakes of Table 2, scaled to comply with the design spectrum, as described previously. According to Figure 13, maximum displacements arise at different timing and different excitations. For instance, seismic event 6 of Table 2 leads to the maximum displacement for the horizontal north–south excitation shown in Figure 13b. For the vertical loading direction (Figure 13c), seismic event 5 of Table 2 seems to cause the highest displacement.

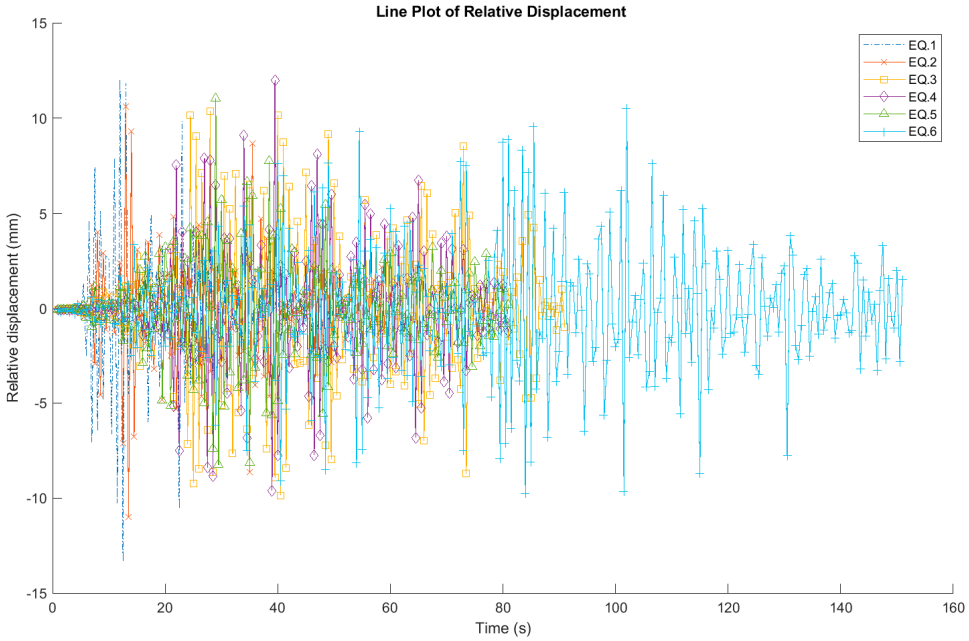

(**a**)

Figure 13. *Cont.*

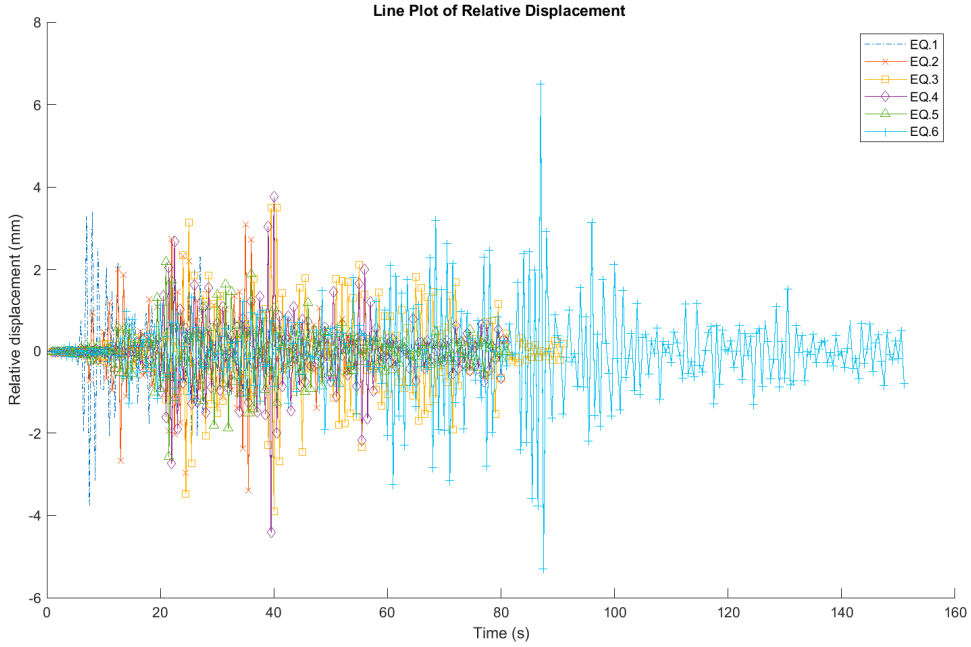

(**b**)

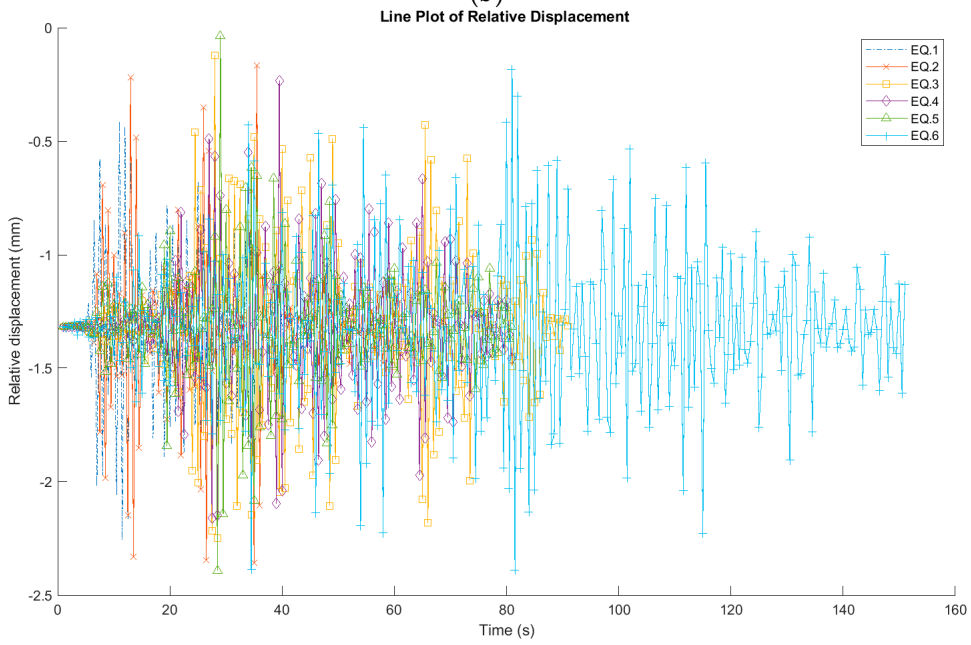

(**c**)

Figure 13. Displacement plots for the first six earthquakes at a point of vault four: (**a**) horizontal east–west displacement component; (**b**) horizontal north–south displacement component; (**a**,**c**) vertical displacement component.

Diagrams comparing the maximum values of the displacements calculated from time history analysis and the displacements obtained from spectral analysis for the selected points are provided in Figures 14–17. The names and numbering of the structural elements correspond to the ones given in Figure 6. Namely, with FW and BW, the front and back walls are named, V denotes the centers of the vaults (seven vaults) and W denotes the upper points of the internal walls, as shown in Figure 6.

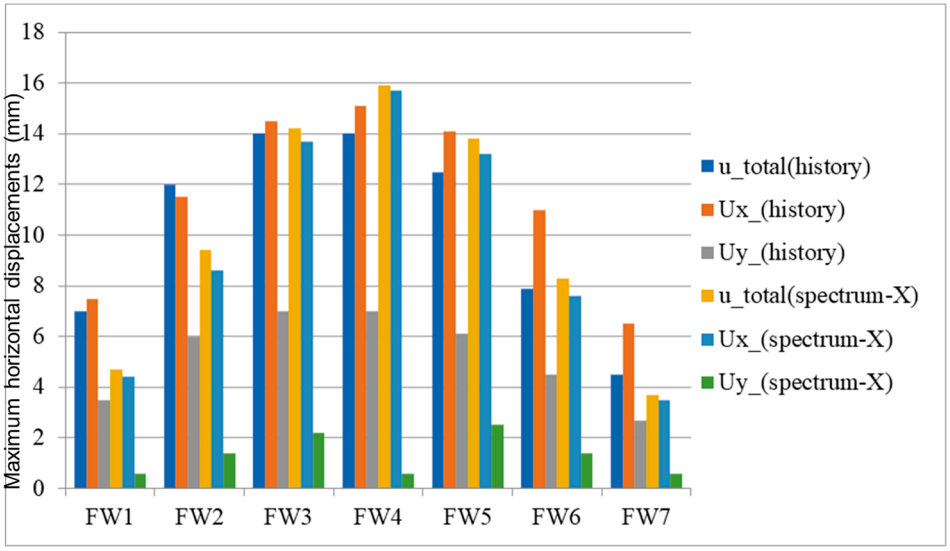

Figure 14. Maximum horizontal displacements (mm) for all earthquakes obtained from time history and response spectrum analysis, at the central point of the vaults.

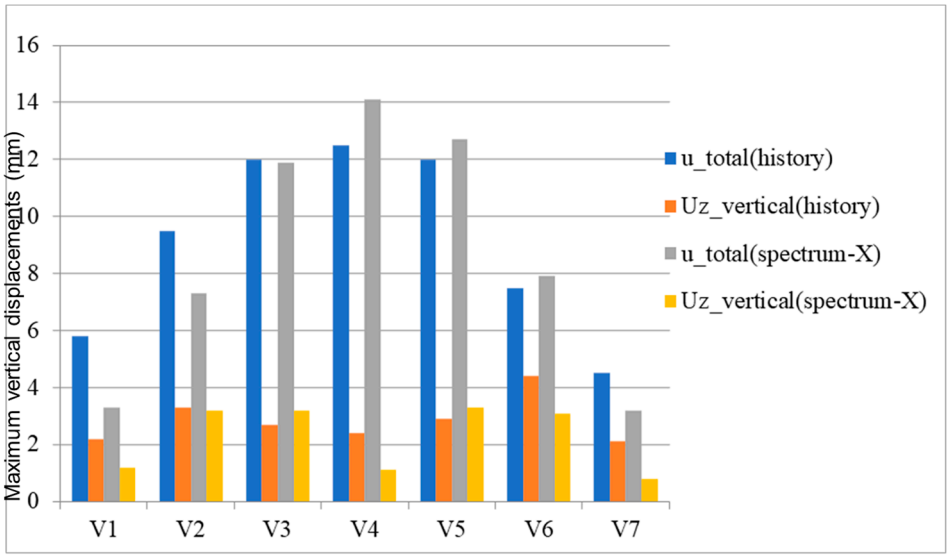

Figure 15. Maximum vertical displacements (mm) for all earthquakes obtained from time history and response spectrum analysis, at the central point of the vaults.

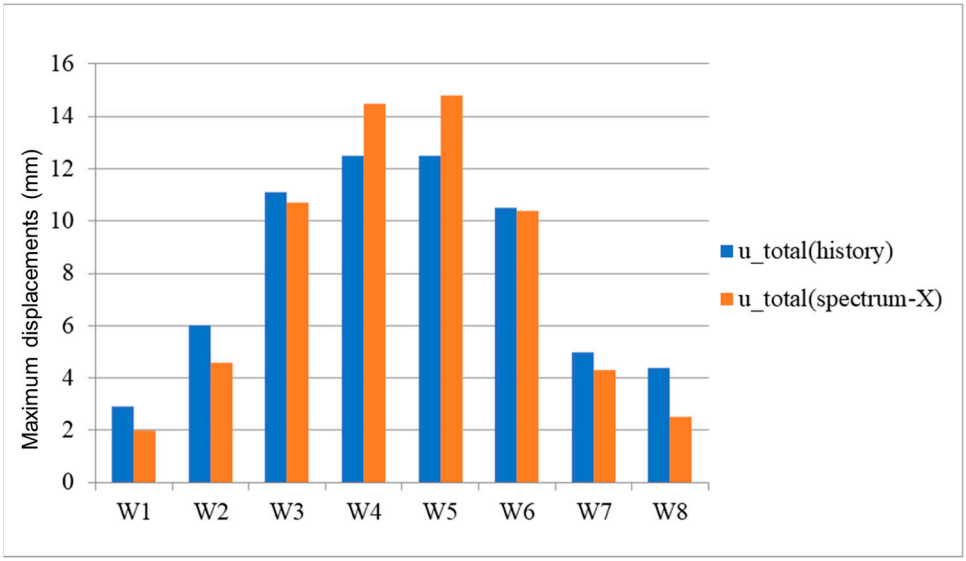

Figure 16. Maximum displacements (mm) for all earthquakes obtained from time history and response spectrum analysis, at the central point of longitudinal walls.

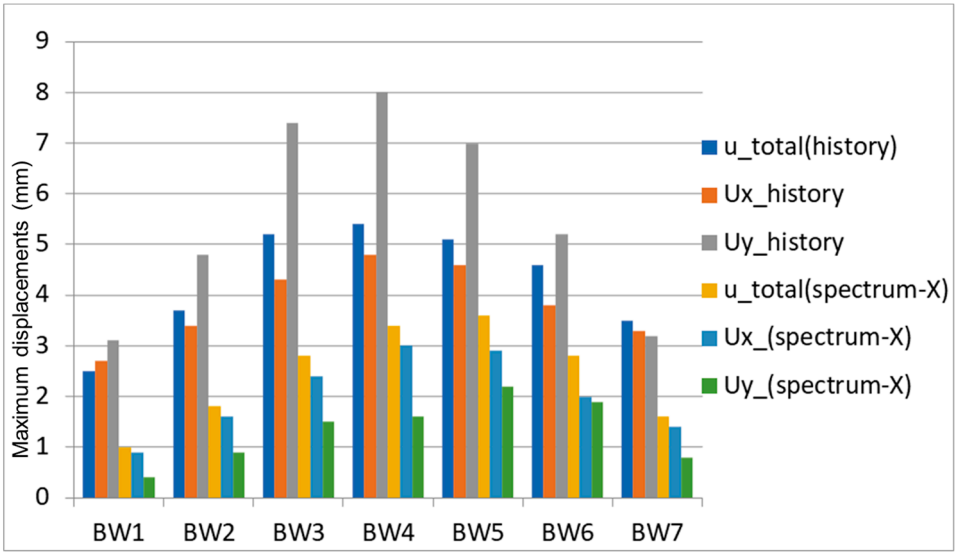

Figure 17. Maximum displacements (mm) for all earthquakes obtained from time history and response spectrum analysis, at the central point of the south wall.

It must be noted that there is a good comparison of the results derived from the two types of dynamic simulations (time history and spectral analysis) at most locations (vaults and longitudinal walls), with a tendency of overestimating the displacement magnitudes at the central vaults obtained from the response spectrum analysis. On the contrary, at the south wall, displacements from the response spectrum analysis were significantly lower as compared to those of the linear history analysis.

3.4. Nonlinear Time History Analysis

Results obtained from nonlinear time history simulations indicate that the building will develop extensive tensile damage in the vaults and the vertical south walls. For both tested seismic events (the Thessaly and the Northridge, California, events shown in Table 2), the maximum failure—as indicated by the tensile damage distribution—is obtained near the maximum (scaled) ground acceleration values, approximately at the fifth and sixth second of the seismic events shown in Figures 7 and 8.

The tensile damage distribution for the two seismic events is provided in Figures 18 and 19, respectively. Both figures depict the initiation of tensile failure, as well as the expansion of failure in the structure. As shown in these figures, the first seismic event develops more intense failure in the five internal vaults. The Northridge seismic event (Figure 19) looks more severe for the two external vaults, as well as for the south vertical walls.

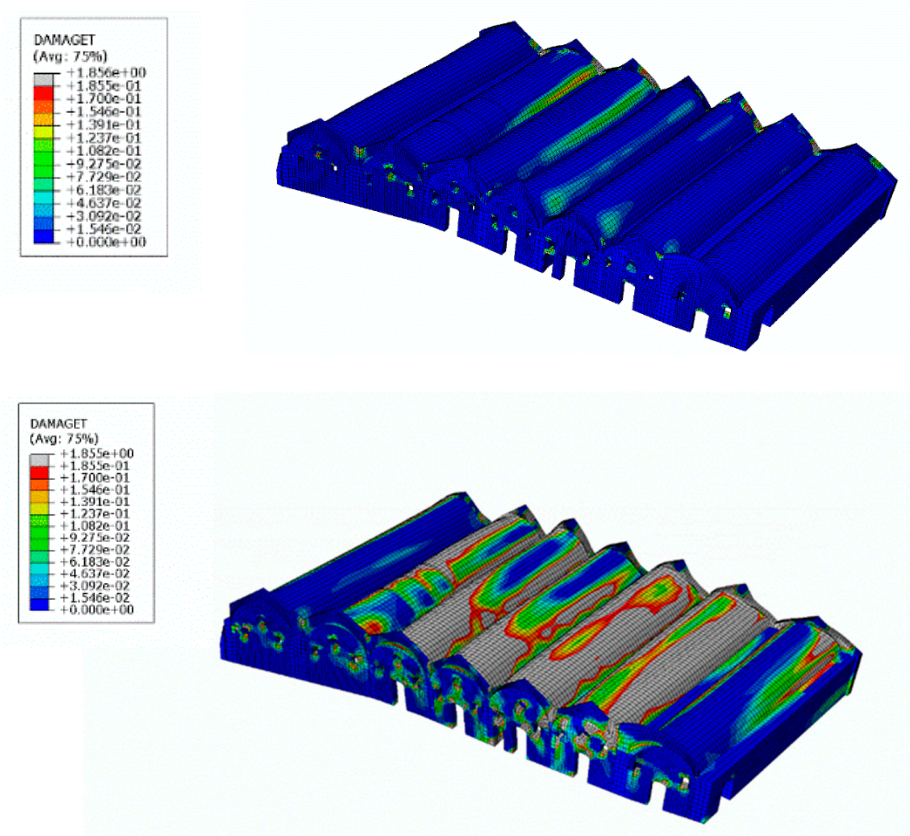

Figure 18. Evolution of the tensile damage distribution during the fifth second of the Thessaly seismic event. Initiation and progress of damage shown in two different time instances.

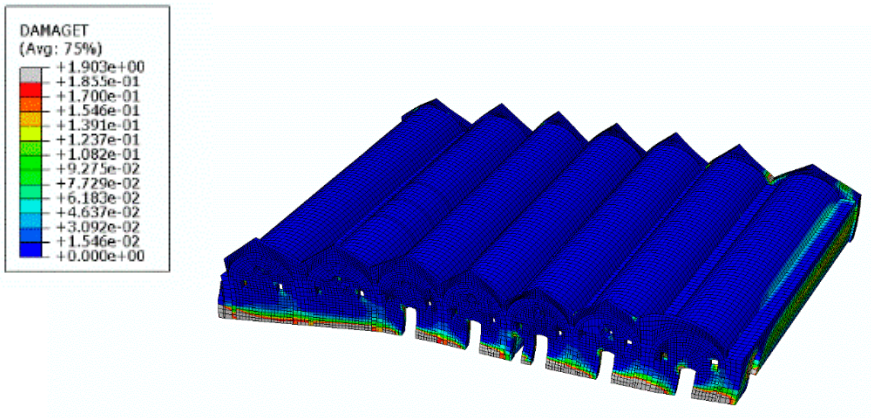

Figure 19. *Cont.*

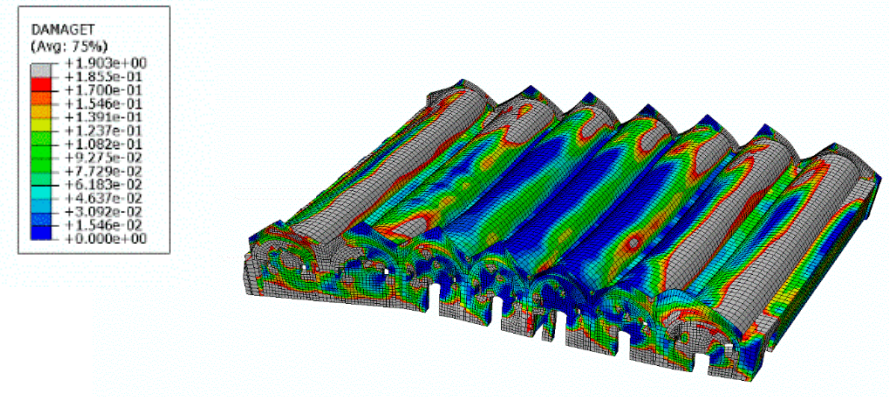

Figure 19. Evolution of the tensile damage distribution during the sixth second of the Northridge. Initiation and progress of damage shown in two different time instances.

4. Discussion

From the previously presented results, it is observed that the comparison of predictions for maximum displacements given by modal analysis and linear time-step analysis is satisfactory. Therefore, design and strengthening techniques based on displacements and deformations of structural elements can proceed with some confidence. Nonlinear analysis is much more complicated. The influence of the material model and of scaling factors for the considered earthquakes requires further investigation. Therefore, for the time being, nonlinear analysis is used for the identification of areas where intervention techniques must be performed more carefully.

The importance of the vertical earthquake component and near fault effects should be emphasized. The study shows the significance of this effect in masonry structures and the need to use reliable computational models. A recent study on seismic collapse probability and life cycle cost assessment of isolated structures subjected to pounding with a smart isolation system using a modified fuzzy-based controller subjected to near-fault earthquakes has been published in [31].

5. Conclusions

For the studied monument, the following conclusions can be drawn. Linear time history analysis gives higher displacements for the vaults and the external walls, while, in general, the predictions are comparable with the spectral analysis technique. Spectral analysis gives much higher estimates for the south wall. Damage estimates coming from nonlinear time history analysis in general agree with the ones coming from linear analysis. Both predict tensile damage in the vaults and the middle, internal walls. Qualitative comparisons of linear and nonlinear models must be evaluated carefully due to an increased amount of material data (strengths, damage parameters, etc.); this is especially needed in the nonlinear cases. When not enough material data is provided by experimental investigation, the results of the nonlinear simulations may not accurately represent the failure response of the structure. Furthermore, the method chosen for the scaling of earthquake records influences the results of nonlinear analysis. All these aspects are, for the time being, open for further investigation. For this reason, the authors propose careful evaluation of the nonlinear analysis results and restricted usage of them.

These findings can be considered to be valid for all monuments that have a relatively complex shape and incorporate both massive and slender structural members, such as the vaults and walls. The analysis justifies the importance of using reliable and accurate geometric models with reliable finite element analysis.

Future research needs are focused in the following two directions:

First, reliable nonlinear material models must be studied and evaluated. In addition, for both linear and nonlinear analysis, the need for reliable scaling of the considered

earthquakes arises. Both elements are crucial to the reliability of the results and their usage for strength estimation.

Second, the creation of reliable reduced order models is necessary in order to facilitate the adoption of the proposed technique from broader engineering practice. In fact, parameter identification tasks, using experimental measurements and parametric analysis and comparison of several intervention measures, require enormous computational resources. Reduced order models could facilitate this task.

Author Contributions: Conceptualization, M.E.S. and G.E.S.; methodology, A.K., B.C., S.M.M., G.A.D., M.E.S. and G.E.S.; software, S.M.M., A.K., B.C., M.E.S. and G.A.D.; validation, M.E.S. and G.A.D.; formal analysis, S.M.M. and A.K. All authors have read and agreed to the published version of the manuscript.

Funding: This research was funded by the Greek Ministry of Culture and Sports, the Municipality of Chania and the Technical University of Crete (Contract ID 20SYMV007057887 21 July 2020).

Data Availability Statement: Selected data of the study are available from corresponding author after justified request.

Conflicts of Interest: The authors declare no conflict of interest.

References

1. Lourenço, P.B. Computations on historic masonry structures. *Prog. Struct. Eng. Mater.* **2002**, *4*, 301–319. [CrossRef]
2. Tzamtzis, A.D.; Asteris, P.G. Finite Element Analysis of Masonry Structures: Part II—Proposed 3-D Nonlinear Microscopic Model. In Proceedings of the Ninth North American Masonry Conference, Clemson, SC, USA, 1–4 June 2003.
3. Penelis, G.; Penelis, G. Restoration of the Margirgis Church and Roman Tower in Cairo. *Struct. Eng. Int.* **2020**, *30*, 64–73. [CrossRef]
4. D'Altri, A.M.; Sarhosis, V.; Milani, G.; Rots, J.; Cattari, S.; Lagomarsino, S.; Sacco, E.; Tralli, A.; Castellazzi, G.; de Miranda, S. Modeling Strategies for the Computational Analysis of Unreinforced Masonry Structures: Review and Classification. *Arch. Computat. Methods Eng.* **2020**, *27*, 1153–1185. [CrossRef]
5. Kappos, A.J.; Penelis, G.G.; Drakopoulos, C.G. Evaluation of simplified models for lateral load analysis of unreinforced masonry buildings. *ASCE J. Struct. Eng.* **2002**, *128*, 890–897. [CrossRef]
6. Quagliarini, E.; Maracchini, G.; Clementi, F. Uses and limits of the Equivalent Frame Model on existing unreinforced masonry buildings for assessing their seismic risk: A review. *J. Build. Eng.* **2017**, *10*, 166–182. [CrossRef]
7. Shabani, A.; Kioumarsi, M.; Zucconi, M. State of the art of simplified analytical methods for seismic vulnerability assessment of unreinforced masonry buildings. *Eng. Struct.* **2021**, *239*, 112280. [CrossRef]
8. Leftheris, B.; Sapounaki, A.; Stavroulaki, M.E.; Stavroulakis, G.E. *Computational Mechanics for Heritage Structures*; WIT-Computational Mechanics Publications: Boston, MA, USA, 2006.
9. Asteris, P.G.; Chronopoulos, M.P.; Chrysostomou, C.Z.; Varum, H.; Plevris, V.; Kyriakides, N.; Silva, V. Seismic vulnerability assessment of historical masonry structural systems. *Eng. Struct.* **2014**, *62*, 118–134. [CrossRef]
10. Da Silva Luis, C.M.; Milani, G.; Paulo, B. Lourenço: Probabilistic-based discrete model for the seismic fragility assessment of masonry structures. *Structures* **2023**, *52*, 506–523. [CrossRef]
11. Bhattacharya, S.; Nayak, S.; Dutta, S.C. A critical review of retrofitting methods for unreinforced masonry structures, International. *J. Disaster Risk Reduct.* **2014**, *7*, 51–67. [CrossRef]
12. Spyrakos, C.C.; Maniatakis, C.A. Nominal Life of Interventions for Monuments and Historic Structures. In *Transdisciplinary Multispectral Modeling and Cooperation for the Preservation of Cultural Heritage. TMM_CH 2018*; Moropoulou, A., Ed.; Communications in Computer and Information Science; Springer: Cham, Switzerland, 2019; Volume 962.
13. Kocaman, İ. Effect of restoration interventions on the seismic behavior of historical masonry buildings: The case of Molla Siyah mosque. *Eng. Fail. Anal.* **2023**, *148*, 107206. [CrossRef]
14. Wu, X.; Lu, J.; Wang, Z.; Yang, W.; Qiao, N. Dynamic characteristics and seismic response analysis of the bottle-shaped masonry ancient pagoda. *Structures* **2022**, *44*, 1648–1659. [CrossRef]
15. Ferrante, A.; Loverdos, D.; Clementi, F.; Milani, G.; Formisano, A.; Lenci, S.; Sarhosis, V. Discontinuous approaches for nonlinear dynamic analyses of an ancient masonry tower. *Eng. Struct.* **2021**, *230*, 111626. [CrossRef]
16. Schiavoni, M.; Giordano, E.; Roscini, F.; Clementi, F. Numerical modeling of a majestic masonry structure: A comparison of advanced techniques. *Eng. Fail. Anal.* **2023**, *149*, 107293. [CrossRef]
17. Sharma, S.; Marasca, A.; Ponte, M.; Bento, R. Modelling the in-plane cyclic behaviour of typical Portuguese rubble stone masonry using the applied element method. *Structures* **2022**, *46*, 1224–1242.
18. Porcu, M.C.; Montis, E.; Saba, M. Role of model identification and analysis method in the seismic assessment of historical masonry towers. *J. Build. Eng.* **2021**, *43*, 103114. [CrossRef]

19. Hoveidae, N.; Fathi, A.; Karimzadeh, S. Seismic damage assessment of a historic masonry building under simulated scenario earthquakes: A case study for Arge-Tabriz. *Soil Dyn. Earthq. Eng.* **2021**, *147*, 106732. [CrossRef]
20. Di Gennaro, L.; Guadagnuolo, M.; Monaco, M. Rocking Analysis of Towers Subjected to Horizontal Forces. *Buildings* **2023**, *13*, 762. [CrossRef]
21. Chácara, C.; Reátegui, R.; Oré, Á.; Suarez, P.; Aguilar, R. Integration of NDT, 3D parametric modelling, and nonlinear numerical analysis for the seismic assessment of a vaulted stone-masonry historical building. *J. Build. Eng.* **2023**, *70*, 106347. [CrossRef]
22. Su, Z.; Zheng, W.; Wang, Y.; Hou, X. Seismic Vulnerability Analysis of Masonry Structures Built with Disassembled Brick Wall Sections. *Buildings* **2022**, *12*, 1831. [CrossRef]
23. Charalambidi, B.; Koutsianitis, P.; Motsa, S.-M.; Tairidis, G.; Kasampali, A.; Drosopoulos, G.; Stavroulaki, M.; Stavroulakis, G.E. Modelling, identification and struc-tural damage investigation of the Neoria monument in Chania. *Dev. Built Environ.* **2022**, *10*, 100069. [CrossRef]
24. Stavroulaki, M.E.; Riveiro, B.; Drosopoulos, G.A.; Solla, M.; Koutsianitis, P.; Stavroulakis, G.E. Modelling and strength evaluation of masonry bridges using terrestrial photogrammetry and finite elements. *Adv. Eng. Softw.* **2016**, *101*, 136–148. [CrossRef]
25. Valente, M. Earthquake response and damage patterns assessment of two historical masonry churches with bell tower. *Eng. Fail. Anal.* **2023**, *151*, 107418. [CrossRef]
26. *Greek Anti-Seismic CODE—2000 (EAK 2000), Earthquake Design and Protection Organization and, Association of Civil Engineers of Greece*; ATTICA PRINTING SA: Athens, Greece, 2000.
27. Valente, M. Seismic behavior and damage assessment of two historical fortified masonry palaces with corner towers. *Eng. Fail. Anal.* **2022**, *134*, 106003. [CrossRef]
28. Tapkın, S.; Tercan, E.; Motsa, S.; Drosopoulos, G.A.; Stavroulaki, M.E.; Maravelakis, M.; Stavroulakis, G.E. Structural Investigation of Masonry Arch Bridges Using Various Nonlinear Finite Element Models. *J. Bridge Eng.* **2022**, *27*, 04022053. [CrossRef]
29. Seismosoft. SeismoMatch 2022—A Computer Program for Spectrum Matching of Earthquake Records. 2022. Available online: https://seismosoft.com/ (accessed on 18 August 2023).
30. Al-Atik, L.; Abrahamson, N.A. An improved method for nonstationary spectral matching. *Earthq. Spectra* **2010**, *26*, 601–617. [CrossRef]
31. Rayegani, A.; Nouri, G. Seismic collapse probability and life cycle cost assessment of isolated structures subjected to pounding with smart hybrid isolation system using a modified fuzzy based controller. *Structures* **2022**, *44*, 30–41. [CrossRef]